Proceedings of International Conference on Heat Exchanger Fouling and Cleaning VIII - 2009 (Peer-reviewed)
June 14-19, 2009, Schladming, Austria
Editors: H. Müller-Steinhagen, M.R. Malayeri and A.P. Watkinson

PRECIPITATION FOULING ON VARIOUS AUSTENITIC ALLOYS

A. Al-Janabi [1], M.R. Malayeri [1], H. Müller-Steinhagen [1,2] and O.O. Badran[3]

[1] Institute for Thermodynamics and Thermal Engineering (ITW), University of Stuttgart
Pfaffenwaldring 6, D-70550, Stuttgart, Germany, herz@itw.uni-stuttgart.de
[2] Institute for Technical Thermodynamics, German Aerospace Centre (DLR), Pfaffenwaldring 38-40, D-70569, Stuttgart, Germany
[3] Faculty of Engineering Technology, Al-Balqa` Applied University, Amman, Jordan

ABSTRACT

The present work endeavours to investigate experimentally the performance of various austenitic alloys such as SMO254 and hastelloy C-276 during forced convective precipitation fouling of supersaturated $CaSO_4$ solutions. For comparison purposes, standard stainless steel and gold coated surfaces are also investigated under similar operating conditions. The theoretical Lewis acid-base approach of surface energy is used to characterise fouling performance of these surfaces. The experimental results show that the surfaces have qualitatively the same fouling trend in terms of fouling resistance except for the gold coated surface which showed that the deposit layer is spalled off the surface along with sporadic flake-off of the coating layer resulting in numerous corroded spots on the surface. Such phenomenon has not been observed for the SMO254 and C-276 surfaces. Surfaces with lower electron donor component (γ_s^-) of the surface energy, e.g. SMO254 surfaces, are more prone to fouling. This is because low γ_s^- increases the attractive interaction energy between the surface and deposits. For such surfaces, this leads to undesired increase of the fouling rate in comparison to that of AISI 304 BA and C-276 substrates.

INTRODUCTION

Metals e.g. stainless steel in various types and alloys are widely used for the construction of heat exchangers. The preference in selection of different metals/alloys is primarily based on their resistance to corrosion. However, it is questionable whether, along with reduction in corrosion, these alternative metals may also reduce fouling. This is because one major driving force for precipitation fouling is the temperature gradient between the surface and bulk which still leads to fouling even in the presence of anti-corrosive surfaces.

The formation of deposits primarily leads to a deterioration of heat transfer due the additional thermal resistance. The secondary impact of fouling may be in-situ corrosion which can occur on the surface next to the deposit crystals if an electron charge difference with the substrate exists. Once corrosion begins, the metal surface will form corrosion products e.g. iron oxide flakes and particles. The presence of suspended corrosion products may cause further deposition downstream. Accordingly, alloys that are essentially immune to fouling and corrosion simultaneously are of great interest to the industry.

Förster and Bohnet (1999), Gao et al. (2006) and Geddert et al. (2007) investigated the behaviour of various metallic and non-metallic surfaces subjected to precipitation fouling. They analyzed the results based on the influence of surface energy as it gives a direct measure of interfacial attractive forces between the surface and deposit. Förster and Bohnet (1999) and Geddert et al. (2007) demonstrated that copper and brass alloyed substrates generally foul more than stainless steel due to i) the effect of corrosion (Somerscales, 1999) and ii) higher surface energy (Tyson, 1975; Förster and Bohnet, 1999). Contrariwise for aluminum, though having lower surface energy than that of stainless steel, a higher deposition rate than for stainless steel was observed. This has been related to the rapid deterioration and loss of surface material (i.e. oxidization) which could imply a change in initial surface energy (Förster and Bohnet, 1999).

In the meantime, AISI 300 series stainless steels i.e. AISI 304 and AISI 316 are still extensively utilized as materials for manufacturing of heat exchangers. On the outer surfaces of these metals a thin layer of Cr_2O_3 is instantly formed when exposed to an oxidizing atmosphere such as air. This oxide layer protects the base material against corrosion. However, if this protective film is damaged locally, the base metal becomes prone to corrosion, particularly in aqueous salt solutions. To prevent this, AISI stainless steel alloys can be fortified by incorporation of small amounts of Molybdenum and Nickel, such as SMO254 and C-276 alloys.

The present work aims to discern the influence of the austenitic stainless steel alloys (SMO254 and C-276) on the deposition process from supersaturated calcium sulphate solutions at a given bulk temperature of 40°C, a flow velocity of 0.15 m/s and a $CaSO_4$ concentration of 4 g/L. The subsequent analysis of the experimental results highlights the conditions where the electron donor component of surface energy would most influence the deposition process.

2. MATERIAL AND METHODS

2.1 Heat transfer substrates and specimens

The heat transfer substrates investigated in this study are as follows:

i) high-grade AISI 304 BA stainless steel sheet with a thickness of 0.3 mm.
ii) high-alloyed austenitic stainless steel (SMO 254) with a thickness of 0.6 mm.
iii) high-alloyed austenitic stainless steel (hastelloy C-276) with a thickness of 0.6 mm.
iv) gold coated AISI 304 BA plates with a thickness of 0.3 mm.

The compositions of the alloyed austenitic substrates which have high contents of molybdenum and nickel are listed in Table 1, and some physical properties in Table 2.

Table 1. Chemical composition of substrates.

Surface	Typical composition, weight %				
	C	Cr	Mo	Ni	Others
AISI 304 BA	0.08	20	---	10.5	69.42
SMO254	0.01	20	6.1	18	55.89
C-276	0.02	15	16	60	8.98

Table 2. Physical properties of substrates.

Mechanical and physical properties	AISI 304 BA	SMO254	C-276
Density, g/cm^3	8.030	8	8.9
Elastic modulus, GPa	193	195	205
Specific heat, J/kg/K	503	485	425
Thermal conductivity, W/m K	18	13.5	10.2

Figure 1 shows a schematic drawing of the heat transfer specimens. Substrates (AISI 304 BA, SMO 254, hastelloy C-276 and gold plated stainless steel) in form of thin plates are vacuum-soldered to two copper blocks (40 mm × 20 mm × (10 and 15) mm). The copper blocks are used to determine the transmitted heat flux via the temperature difference in perpendicular direction. Six thermocouples are inserted in these copper blocks to measure the temperature gradient. This arrangement facilitates the investigation of various substrates and coatings. Two 450 Watt golden infrared heaters (Heraeus Noblelight GmbH, Hanau, Germany) are also used to provide the required heat flux.

2.2 Surface roughness

The surface roughness of all surfaces was measured by using a stylus device. The widely used roughness parameter "mean roughness profile (R_a)" is considered which ranges from 0.12 to 0.18 μm. It has been found that, the surface roughness within this range will most likely not impact the fouling process (Yoon and Lund, 1994; Santos et al., 2003). It is therefore plausible to ignore the effect of surface roughness on fouling mechanisms in this work.

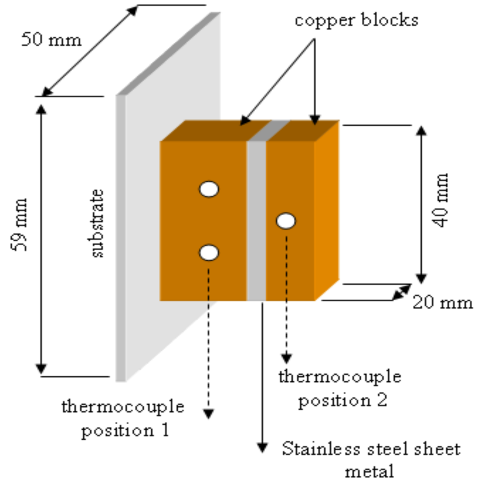

Fig.1 Heat transfer specimen.

2.3 Surfaces energy

There is no direct method to determine the surface energy of solids other than through measurements of contact angle combined with an appropriate theoretical approach. Among several available approaches the acid-base method appears to be convenient for systems involving aqueous media. This approach was developed by van Oss et al. (1986, 1988) and assumes that the total surface energy of a solid is the sum of a non-polar Liftshitz-van der Waals (LW) component γ^{LW}, and a polar Lewis acid/base component γ^{AB}:

$$\gamma_i = \gamma_i^{LW} + \gamma_i^{AB} \tag{1}$$

The acid-base polar component can be further subdivided into electron donor and electron acceptor interactions components:

$$\gamma_i^{AB} = 2\sqrt{\gamma_i^+ \gamma_i^-} \tag{2}$$

The solid/liquid interface energy is then given by

$$\gamma_{sl} = \gamma_s + \gamma_l - 2(\sqrt{\gamma_s^{LW} \cdot \gamma_l^{LW}} + \sqrt{\gamma_s^+ \cdot \gamma_l^-} + \sqrt{\gamma_s^- \cdot \gamma_l^+}) \tag{3}$$

The combination of Eq. (3) and Young Eq. (4) (Young, 1805) yields a relation between the measured contact angle and the solid and liquid surface free energies as:

$$\gamma_{sl} = \gamma_s - \gamma_l \cos\theta \tag{4}$$

$$\gamma_l \cdot (1 + \cos\theta) = 2(\sqrt{\gamma_s^{LW} \cdot \gamma_l^{LW}} + \sqrt{\gamma_s^+ \cdot \gamma_l^-} + \sqrt{\gamma_s^- \cdot \gamma_l^+}) \tag{5}$$

The experimental procedure for the determination of surface components γ_s^{LW}, γ_s^{+} and γ_s^{-} has been described by Good et al. (1991). There are two methods to utilize Eq. (5): i) to measurer the contact angle of three polar liquids with known values of γ_l^{LW}, γ_l^{+} and γ_l^{-} or ii) using only one non-polar liquid for finding γ_s^{LW} and two other polar liquids to obtain γ_s^{+} and γ_s^{-}. In this study, diiodomethane is used as a non-polar liquid, and distilled water and ethylene glycol as polar liquids.

For the measurement of contact angel a Drop Shape Analysis (DSA) is utilized. Prior to the measurements, the surfaces have to be ultrasonically cleaned by acetone and distilled water in sequence. Afterwards, a droplet of a test liquid is placed on the surface under controlled room temperature. The drop image is then recorded by a video camera and displayed on a monitor. Once stabilized, a frozen picture of the droplet will be taken and the contact angle measured using the DSA program, with an accuracy of ±0.1°. Table 3 lists the surface tension components of these liquids (Good, 1992; van Oss et al., 1988). Figure 2 depicts the surface energy values of the investigated specimens. Among the various surface energy components, the most distinguishable factor is the electron donor component (γ_s^{-}).

Table 3. Surface tension components of the test liquids.

Liquids	Surface tension components, mNm^{-1}			
	γ_l^{LW}	γ_l^{+}	γ_l^{-}	γ_l
Water	21.8	25.5	25.5	72.8
Ethylene glycol	29.0	1.92	47	48.0
Diiodomethane	50.8	0	0	50.8

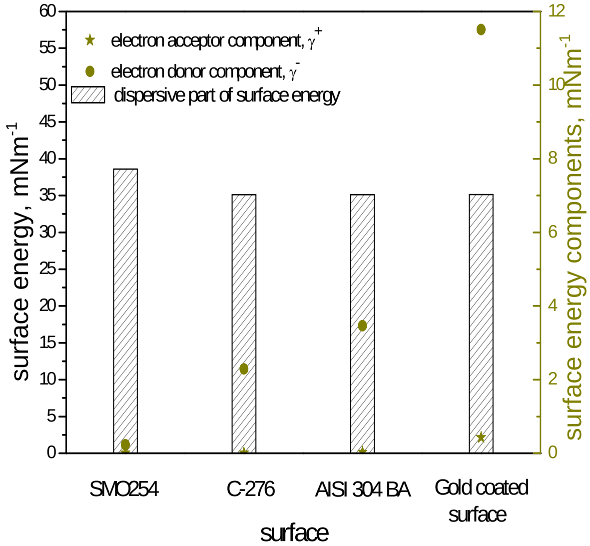

Fig. 2 Surface energy components of investigated substrates.

3. EXPERIMENTAL SET-UP AND PROCEDURE

3.1 Test rig

The investigation of the specimens under clean and fouling conditions is performed using the experimental apparatus presented in Figure 3. The closed loop set-up consists of two identical test sections operated in parallel. Each test section is a vertical rectangular duct with a dimension of (39mm x 13mm x1670 mm). On both wide sides of each duct, openings with a dimension of 59 mm x 50 mm exist where the specimens (see Fig. 1) can be mounted. The heated zone of the specimen is positioned 1.5 m upstream from the inlet of the ducts to allow the hydraulic flow to be fully-developed. By using a centrifugal pump [2], the solution is pumped from a 47 liter stainless steel tank [1] through a filter [3] to remove any broken crystals and impurities from the solution, which might artificially act as nucleation sites. The filter has 12 µm pore size, is 0.5 m long and made of polypropylene and polyethylene (Rizzo, 2008). After the filter, the main flow is divided into two equal streams which flow into the left and right test sections. Afterwards the two streams are recombined and fed back to the storage tank for being recirculated again. The maximum flow rate for both measuring sections corresponds to a Reynolds number of approximately 12,950. The temperature of the solution in the tank was regulated by an adjustable water cooled coil, together with two heater pads [7] installed on the outer surface of the tank.

3.2 Determination of the surface temperature

The surface temperature is measured by K-type (Ni-Cr / Ni-Al) thermocouples placed in copper blocks as shown in Figure 1, and determined as:

$$T_s = T_{th} - \frac{\dot{q}\,x}{k} \qquad (6)$$

In Equation (6) the thermal resistance “x/k” between the measuring point of the thermocouples (position 1 in Figure 1) and the heating surface should be obtained. Although the distance between the thermocouple and the heat transfer surface is known, the determination of x/k is not quite simple due to the changing thermal conductivity arising from the presence of the soldering material. Hence, the Wilson Plot procedure is preferred for experimental determination of the x/k values.

3.3 Test solution

Pure calcium sulphate is an inversely soluble salt, with very low solubility in distilled water. For the experiments, the calcium sulphate solution is prepared by mixing an aqueous calcium nitrate tetrahydrate ($Ca(NO_3)_2{\cdot}4H_2O$) solution with an aqueous sodium sulphate (Na_2SO_4) solution in such a way that the desired $CaSO_4$ concentration is finally obtained, see equation (7). These two chemicals are chosen because their higher solubility in water could provide a high enough concentration of foulant ions in the solution (Najibi et al., 1996). In addition, sodium nitrate is highly soluble in water thus the presence of NO_3^- and Na^+

ions in the solution increases the solubility of calcium sulphate (Rizzo, 2008). This can be attributed to the electrostatic attraction between the sodium nitrate ions and the ions with opposite charge formed by calcium sulphate (Marshall et al., 1964). The two chemicals are initially dissolved separately in 23.5 liters of distilled water and heated up to the final bulk temperature of 40°C. Afterwards they are mixed thoroughly for approximately two hours under constant temperature to ensure homogeneity.

$$Ca(NO_3)_2.4H_2O + Na_2SO_4 \rightarrow CaSO_4 + 2NaNO_3 + 4H_2O \quad (7)$$

A visual examination has been done to ensure whether turbidity occurred or not. Liquid turbidity is a clear indication of precipitation. This arises particularly from a very high supersaturation at elevated bulk temperatures. If turbidity occurred then the experiment should be terminated and be set for a new solution.

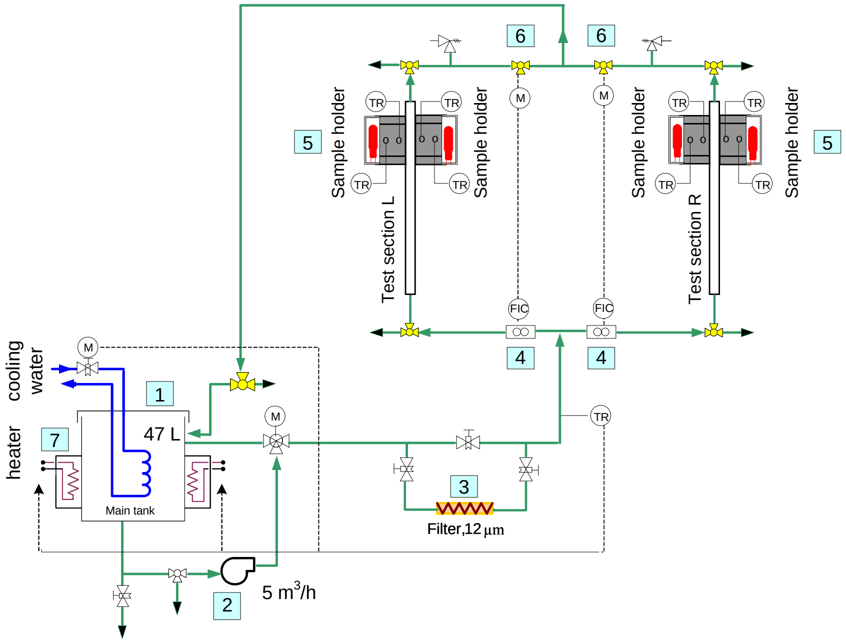

Fig. 3 Schematic diagram of the experimental set-up.

3.4 Determination of calcium sulphate concentration

Once the mixing of salt solutions is accomplished, the calcium concentration is determined by measuring the calcium ion concentration by potentiometric EDTA (Ethylene-Diamine-Tetra-Acetic Acid) titration (Fritz and Schenk, 1987). The stoichiometric reaction is as follows:

$$\left(Ca + Indic^{-}\right) + H_2Y^{2-} \rightarrow CaY^{2-} + H\,Indic^{2-} + H^{+} \quad (8)$$

The titrant (H_2Y^{2-}) is a solution of the disodium salt of EDTA (disodium dihydrogen ethylene-diamine-tetra-acetate). Its concentration was 0.01 mol/L. Eriochrome Black T is used as the indicator and a certain amount of magnesium sulphate ($MgSO_4$) is added at the same concentration as the titrant (H_2Y^{2-}), so that the added amount of magnesium is subtracted from the total EDTA consumption. The pH value of the titration sample has to be adjusted to a value of 9-10 by adding 2-3 ml of ammonia buffer solution with pH=10.

3.5 Clean and fouling heat transfer coefficients

Each individual surface specimen is initially cleaned by toluene to remove any contamination and then immediately mounted into the test rig. Afterwards the selected heat flux, bulk temperature and fluid velocity are adjusted and the rig started to operate under clean conditions with distilled water until steady-state is reached. This is reached when the surface temperature remains constant. During this period the test solution is prepared and heated to the desired bulk temperature. If the surface temperature of all specimens and the other test conditions are stable for more than two hours, the test run is stopped , the distilled water removed and replaced by the test solution. The solution is then circulated for about 10 min with the heaters still off, to ensure that any dissolved air can find its way to deaerators and leave the system. Afterward, the power supply to the test sample is switched on and the data collection started.

During the experiment the Ca^{2+}-ion concentration is determined by EDTA-titration every 2-3 hours and adjusted by manually adding equimolar calcium nitrate tetrahydrate and sodium sulphate to maintain a constant $CaSO_4$ concentration. As soon as the surface temperature of a specimen exceeded a set value, the respective heating is switched off. After the runs, all heating lamps are switched off and the control software stops the test rig automatically and stores all measured data in an output file.

3.6 Error analysis

The error of the experimental results in this study is estimated with 95% confidence as given by Equation (9).

$$U = \left[B^2 + P^2\right]^{1/2} \tag{9}$$

The uncertainty of any experimental data point is a combination of the systematic error (Bias limit, B) and the random error (precision limit, P) (Kline and McClintock, 1953). Systematic experimental errors in this study are due to i) error of approximately ± 0.2°C in temperature measurement and ii) error of about 4.8% for the determination of the heat flux as a result of systematic errors in the measurements of electrical current and voltage. The uncertainty of the fouling resistance varies with time due to changes in surface temperature when deposits start to build up on the heat transfer surfaces. For instance, the uncertainty of the fouling resistance at the initial stage was 15-35%, while it was only 5% in the asymptotic region. This indicates that the largest experimental uncertainty of the fouling resistance occurs during the initial phase of all runs when the temperature difference between wall and fluid is still small.

4. RESULTS AND DISCUSSION

4.1 Fouling resistance

Figure 4 illustrates how the fouling resistances varied as a function of time for two investigated alloys, and for the stainless steel substrate. All surfaces follow similar fouling trends, that is that the fouling resistance starts to increase after a certain period of time (known as the induction time) during which hardly any change in fouling resistance has been observed. Both, the AISI 304 BA and the hastelloy C-276 substrates have approximately the same induction time of 165 minutes. For the SOM254 substrate, however, a significantly prolonged induction time is observed which is almost 3-times that of the AISI 304 BA substrate.

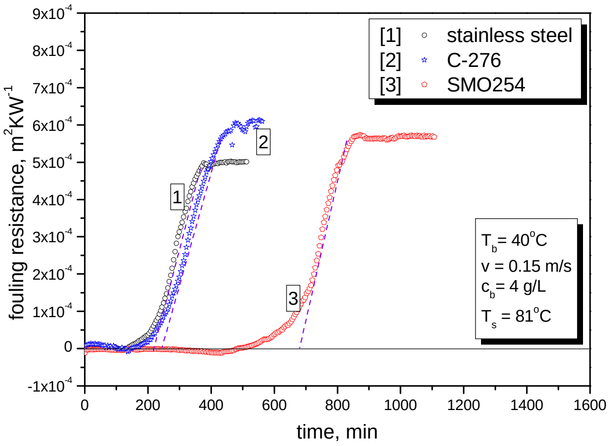

Fig. 4 Fouling resistance as a function of time for alloys and stainless steel surfaces.

In addition, fouling curves trend to level off after some period of operation. There are some differences in the asymptotic values. For instance, the SMO254 substrate shows a 13% higher asymptotic fouling resistance in comparison to the AISI 304 BA steel surface, while only a marginal difference exists between the SMO254 and the C-276 substrates. It may be assumed that the asymptotic fouling resistance is proportional to the deposit thickness. This is clearly validated by visual examination of the fouled surfaces as presented in Figure 5. The variance of the fouling layer thickness over the surface is expected, since the level of turbulence at the upper end of the plate is significantly higher than at the lower end, due to the reduction of cross-sectional flow area. The deposits in all three cases are coherent solid scales with strong adhesion to investigated surfaces

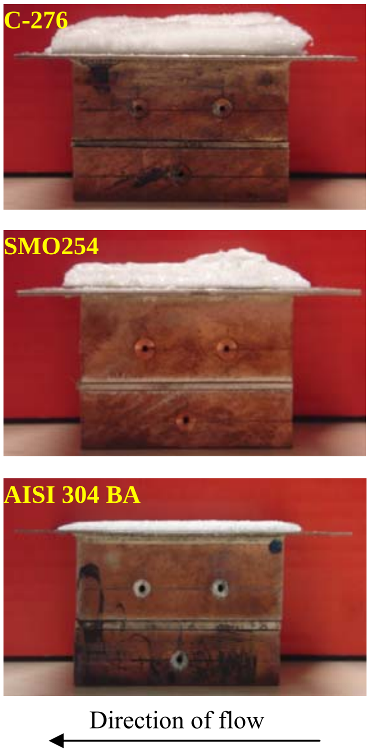

Fig. 5 Fouled surfaces.

In addition, a gold coated surface has been investigated for sake of comparison with the stainless steel and the alloyed metallic substrates. The influence of the gold coated surface on the fouling resistance is illustrated in Figure 6. Apparently, the fouling resistance of the gold coated surface behaves differently. During the first 200 minutes of the run, both fouling rate and fouling resistance are higher than the values observed for stainless steel. After approximately 250 minutes, the deposit layer on the gold coated surface spalled off the surface, followed by a second deposition process with a fouling rate almost similar to that of the initial stage. However, after 600 minutes the fouling resistance decreased rapidly down to zero. Then, another third deposition process occurred with

90% reduced fouling rate compared with the initial fouling rate, reaching an asymptotic value after approximately 800 minutes.

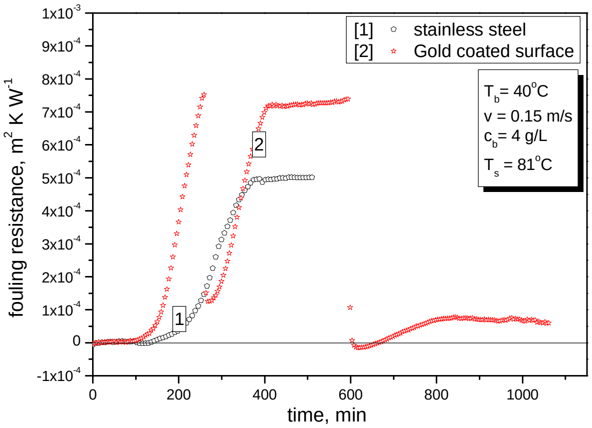

Fig. 6 Fouling resistance as a function of time for the gold coated surface comparison with stainless steel substrate.

The fouling behaviour of the gold coated surface is probably due to the deterioration of the coating layer that could detach the deposits from the surface. This may be hypothesized after inspection of Figure 7, from which it is evident that a large portion of the coating layer is damaged and only little deposit remains on the surface. Hence the removal of the deposit is not solely due to the effect of surface energy, but the coating itself may have taken away part of the deposit while it becomes detached from the substrate. It was observed additionally that the deterioration of the coating layer makes the surface more vulnerable to corrosion and erosion as quite a number of oxidized areas (encircled regions in Fig. 7) have been observed next to the gold coating layer.

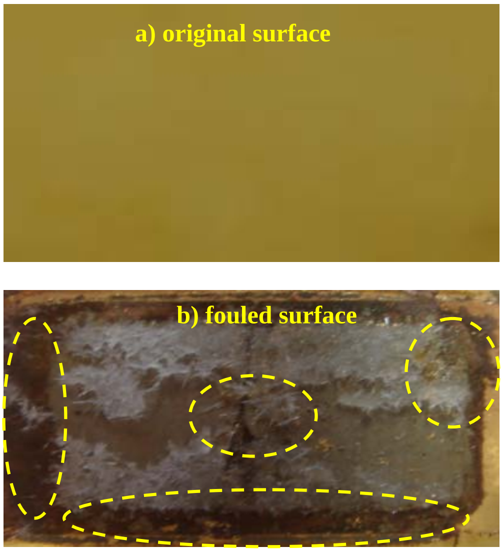

Fig. 7 Pictures of gold coated surface: a) original surface before fouling run and b) fouled surface.

4.2 Evaluation of surface energy impacts

For all investigated surfaces, different affinity to deposit nucleation has been observed. The tendency of surfaces to grow calcium sulphate deposits can also be characterized in terms of fouling rate. The initial fouling rate is defined as the more or less linear slope of a line during progressive change from the end of induction to the beginning of the horizontal region of the fouling curves (as shown in Fig. 4, dash lines). From Figure 8, it can be seen that the variation in fouling rate cannot be related to the effect of the total surface energy. This is because the C-276 and AISI 304 BA surfaces have approximately the same value of γ_s while they show different fouling rates which are 3.02 m^{2}K W^{-1}min^{-1} and 3.15 m^{2}K W^{-1}min^{-1}, respectively. This highlights the insufficiency of the total surface energy to interpret the fouling propensity of these substrates. The results of the gold coated surface are not added in this figure due to damage of the coating layer.

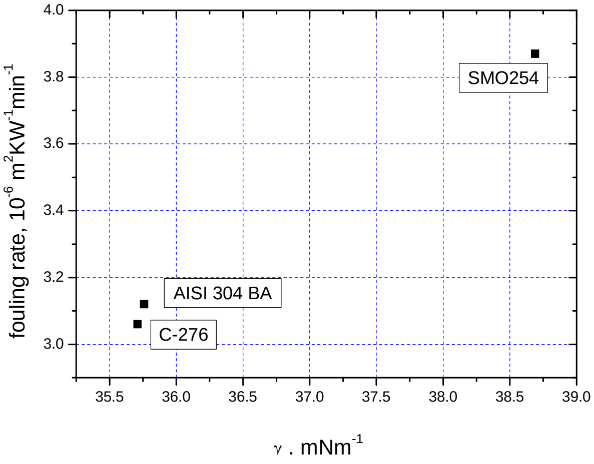

Fig. 8 Fouling rate as a function of the total surface energy for alloys and stainless steel surfaces.

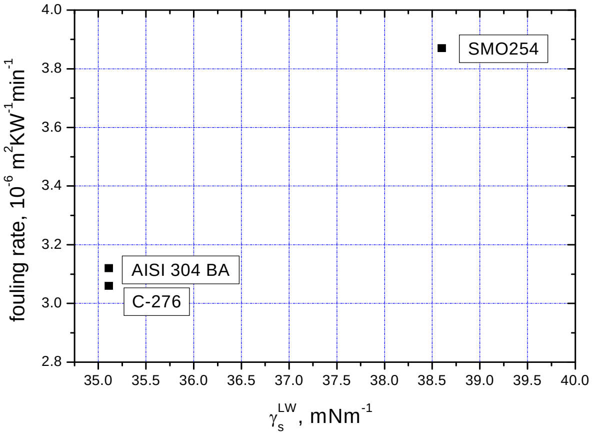

Fig. 9 Fouling rate as a function of the Lifshitz-van der Waals component for alloys and stainless steel surfaces.

The comparison of fouling rates with the Lifshitz-van der Waals component (γ_s^{LW}) as shown in Figure 9 indicates that no clear-cut tendency is evident since different affinity to fouling has occurred for C-276 and

AISI 304 BA surfaces at approximately the same γ_s^{LW} values.

However, comparison of the fouling rates with the electron donor components yield a better correlation. In Figure 10, surfaces with low γ_s^- are more susceptible to fouling as a result of strong attractive energy between the deposits and the heat transfer surface. Although the γ_s^- value of AISI 304 BA is higher than that of C-276 its fouling rate seems to be a slightly (5%) higher compared to the C-276 surface. The authors have no explanation for this trend and further investigation such as repeatability tests are required to confirm the results.

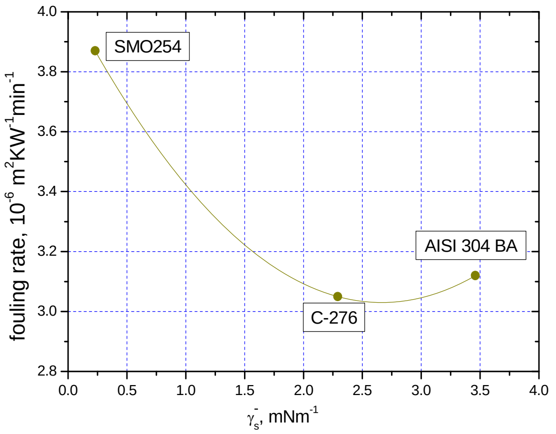

Fig. 10 Fouling rate versus the electron donor component of the surface energy for alloys and stainless steel surfaces.

4.3 Deposit's morphology

Figure 11 depicts two typical SEM pictures for SMO254 and C-276 substrates. The pictures were taken from deposit layer formed from 4 g/L salt solutions for a heat flux of 100 kW/m^2, using SEM (MIRA-II LMH-IB, with a magnification range between 4x and 1,000,000 x). It can be seen that the structure of calcium sulphate is significantly influenced by the substrates. The deposit structure in terms of size and crystal arrangement of SMO254 is entirely different to that on C-276. Large size, thickness and horizontal orientation are the main characteristics of the deposit morphology for SMO254, while thinner crystals with different orientation were observed for C-276. In general, crystals for SMO254 surface are denser, harder, and more adherent than those for the C-276 surface.

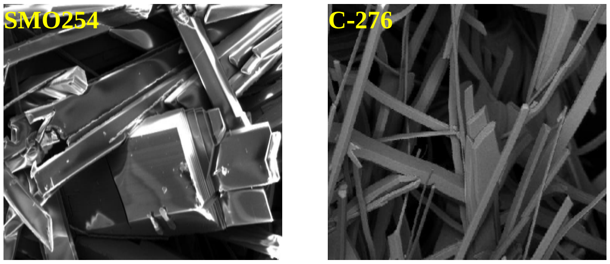

Fig. 11 SEM pictures of $CaSO_4$ deposit formed on the metallic alloys SMO254 and C-276 (size of SEM pictures is 500 µm).

5. CONCLUSIONS

Results presented this paper show how precipitation fouling develops on various austenitic alloys that are frequently used for manufacturing industrial heat exchangers. For the sake of comparison, standard stainless steel and a gold coated surface have also been investigated under identical severe fouling conditions of calcium sulphate. The experimental results showed that all surfaces have similar fouling trends, except for the gold coated surface. Examination of the results also revealed that for investigated materials the electron donor component is an appropriate parameter among various components of total surface energy for characterizing fouling behavior on various materials Surfaces with lower electron donor components, e.g. SMO254, are more susceptible to fouling. This is because a lower electron donor component is indicative of stronger attractive interaction between the surface and the deposits. Post-fouling surface analyses show that the crystalline structure of the deposits on the surfaces differs considerably, with larger, thicker, harder, and more adherent crystals found for SMO254.

ACKNOWLEDGEMENTS

The authors gratefully acknowledge the financial support of the MEDESOL Project (European project, Contract no. 036986). The cooperation of API Schmidt-Bretten GmbH & Co. KG, Germany, by providing SMO254 and C-276 substrates is highly appreciated. The first author also wants to thank the DAAD, "German Academic Exchange Service" for a PhD research studentship.

Nomenclature

B	bias limit
c	concentration, g/L
k	thermal conductivity, W/mK
P	precision limit
R_a	mean roughness profile, µm
R_f	fouling resistance, m^2 K W^{-1}
T	temperature, °C
t	time, min
U	uncertainty
v	velocity, m/s

Greek symbols

γ^{AB}	Lewis acid/base surface energy, mNm^{-1}
γ^{LW}	Lifshitz-van der Waals surface energy, mNm^{-1}
γ_{sl}	solid/liquid surface energy, mNm^{-1}
γ_s	solid surface energy, mNm^{-1}
γ_l	fluid media surface tension, mNm^{-1}
γ^-	electron donor component of surface energy, mNm^{-1}
γ^+	electron acceptor component of surface energy, mNm^{-1}
θ	contact angle, degree

Subscript

b	bulk
s	surface
th	thermocouple

Abbreviations

AISI	American Iron and Steel Institute
$CaSO_4$	calcium sulphate anhydrite
DSA	Drop Shape Analysis
EDTA	Ethylene-Diamine-Tetra-Acetic Acid
SEM	Scanning Electron Microscope

REFERENCES

Förster, M., and Bohnet, M., 1999, Influence of the interfacial free energy crystal/heat transfer surface on the induction period during fouling. *International Journal of Thermal Science*, Vol. 38, pp. 944-954.

Fritz, J. S., and Schenk, G. H., 1987, *Quantitative analytical chemistry*, 5th edition, Allyn and Bacon Inc., USA.

Gao, M., Sun, F., Shi, Z., Lei, S., and Niu, Z., 2006, Experimental research and theoretical analysis of anti-fouling characteristics on the surface of Ni-based implanted tube, *International Communications in Heat and Mass Transfer,* Vol. 33, pp. 1115-1121.

Geddert, T., Kipp, S., Augustin, W., and Scholl, S., 2007, Influence of different surface materials on nucleation and crystal growth in heat exchangers, *proceeding, 7th International Heat Exchanger Fouling and Cleaning*, Tomar, Portugal.

Good, R. J., 1992, Contact angle, wetting and adhesion, a critical review, *Journal of Adhesion Science Technology*, Vol. 6, pp. 1269-1302.

Good, R. J., Chaudhury, M. K., and van Oss, C. J., 1991, Theory of adhesive forces across interfaces 2. Interfacial hydrogen bonds as acid-base phenomena and as factors enhancing adhesion. In: L.H. Lee Editor, *Fundamentals of adhesion* Plenum Press, New York, pp. 153–172.

Kline, S. J., and McClintock, F. A., 1953, Describing uncertainties in single-sample experiments, *Mechanical Engineering*, Vol. 75, pp. 3-8.

Marshall, W., Slusher, R., and Jones, E. V., 1964, Solubility and thermodynamic relationships for $CaSO_4$ in $NaCl-H_2O$ solutions from 40°C to 200°C., 0 to 4 Molal NaCl, *Journal of Chemical and Engineering Data*, Vol. 9, pp. 187-191.

Najibi, S., Müller-Steinhagen, H., and Jamialahmadi, M., 1996, Calcium sulphate scale formation during subcooled flow boiling, *Chemical Engineering Science*, Vol. 52 (8), pp. 1265-1284.

Rizzo, 2008, Induktionszeit beim kristallisations fouling an ionenimplantierten wärmeübertragerflächen. *PhD dissertation*, ITW Institute, Stuttgart University, Germany.

Santos, O., Nylander, T., Rizzo, G., Müller-Steinhagen, H., Trägårdh, C., and Paulsson, M., 2003, Study of whey protein adsorption under turbulent flow, *Heat exchanger Fouling Fundament Approaches and Technical Solutions*, Santa Fe, US.

Somerscales, E. F. C., 1999, Fundamentals of corrosion fouling, *British Corrosion Journal*, Vol. 34 (2), pp. 109-124.

Tyson, W. R., 1975, Surface energies of solid metals, *Canadian Metallurgical Quarterly*, Vol. 14 (4), pp. 307-314.

van Oss, C. J., Good, R. J., and Chaundhury, M. K., 1986, The role of van der Waals forces and hydrogen bonds in 'hydrophobic interactions' between biopolymers and low energy surfaces. *Journal of Colloid Interface Science*, Vol. 111, pp. 378-390.

van Oss, C. J., Good, R. J., and Chaundhury, M. K., 1988, Additive and non-additive surface-tension components and the interpretation of contact angles. *Langmuir* 4, pp. 884-891.

Yoon, J., and Lund, D. B., 1994, Magnetic treatment of milk and surface treatment of plate heat exchangers: effects on milk fouling, *Journal of Food Science* Vol. 59 (5), pp. 964–980.

Young, T., 1805, An essay on the cohesion of fluids. *Philosophical Transactions of the Royal Society*, London.